edited by Joel S. Levine

Biomass Burning and Global Change

VOLUME 1

Remote Sensing, Modeling and Inventory Development, and Biomass Burning in Africa

© 1996 Massachusetts Institute of Technology

All rights reserved. No part of this book may be reproduced in any form by any electronic or mechanical means (including photocopying, recording, or information storage and retrieval) without permission in writing from the publisher.

This book was set in Times Roman on the Monotype "Prism Plus" PostScript Imagesetter by Asco Trade Typesetting Ltd., Hong Kong.
Editorial and production services were provided by Superscript Editorial Production Services.
Printed and bound in the United States of America.

Library of Congress Cataloging-in-Publication Data

Biomass burning and global change / edited by Joel S. Levine.
p. cm.
Includes bibliographical references and index.
ISBN 0-262-12201-4 (vol. 1 : alk. paper). —
ISBN 0-262-12202-2 (vol. 2 : alk. paper)
1. Burning of land—Environmental aspects.
2. Fuelwood—Burning—Environmental aspects.
3. Climatic changes. I. Levine, Joel S.
TD195.B56858 1996
628.5'3—dc20 96-35030
CIP

Contents

Volume 1

Contributors xxiii

Introduction xxxv

Joel S. Levine

I Remote Sensing: Global and Regional Scales

1

Mission to Planet Earth: Land-Cover/Land-Use Change Program 3

Anthony C. Janetos, Christopher O. Justice, and Robert C. Harriss

2

Developing a Global Vegetation Fire Monitoring System for Global Change Studies: A Framework 14

Jean Paul Malingreau and Jean-Marie Grégoire

3

AVHRR Monitoring of Vegetation Fires in the Tropics: Toward the Development of a Global Product 25

Alberto W. Setzer and Jean Paul Malingreau

4

The Simulation of AVHRR Data for the Evaluation of Fire-Detection Techniques 40

Pete Dowty

AVHRR Monitoring of Vegetation Fires in the Tropics: Toward the Development of a Global Product

Alberto W. Setzer and Jean Paul Malingreau

Fire has accompanied and played important roles in the development of the vegetation of our planet. Since its control by humans about half a million years ago, it has been a major tool in hunting, forest conversion, agriculture, and pasture renewal, just to mention a few uses related to vegetation changes. Since the pioneer work of Crutzen et al. (1979) environmental effects resulting from vegetation fires have increasingly become a subject of scientific interest. With tropical deforestation taking place at unprecedented rates, they rapidly changed into a worldwide scientific and public environmental concern. Two recent publications (Levine 1991; Crutzen and Goldammer 1993) contain hundreds of references that extensively document the current importance of biomass burning.

Of particular interest is the estimate of the location and extent of vegetation burning on the planet, which has yet to be made. Supposedly, 60% of the pantropical savannas in the world, about 15×10^6 km^2, may be affected by fire every year (Goldammer 1993). Tropical deforestation, normally attained through the use of fire, was estimated at 15.4×10^4 km^2 for the last decade (Singh 1993); unknown immense areas of boreal forests are also destroyed by fires. On a global basis, carbon emissions from biomass burning could account for 30–80% of the fossil fuel burning rate of 5.7×10^{15} g of carbon per year, with significant effects in biogeochemical cycles and possibly also on the climate (Crutzen and Andreae 1990).

Vegetation fires occur on all continents (e.g., Andreae 1993) and difficulties in their detection with conventional ways for most of the world makes systematic remote sensing from space the only possibility for their comprehensive study. Because of its daily coverage, low (1.1 km) resolution images of the Advanced Very High Resolution Radiometer (AVHRR) aboard the National Oceanographic and Atmospheric Administration (NOAA) series satellites (Kidwell 1991) have been used in thermal detection of active fires in daytime since the early work of Matson and Dozier (1981) pointed to this possibility. An AVHRR-based real-time operational program for firefighting and monitoring has existed for many years on a regional scale (Setzer and Pereira 1991a) and an AVHRR global fire product is under consideration (IGBP 1992) following Malingreau (1990) and Malingreau et al. (1993). However, little validation of AVHRR fire detection algorithms is found in the literature; different authors use different methods and commonly refer to fires detected and mapped without any field verification. More recently Setzer et al. (1994) describe AVHRR responses to two large forest fires in Amazonia, and Belward et al. (1993) to five fires in West African savannas; in opposition to algorithms using a multichannel approach, these data sets indicate that AVHRR's channel 3 (3.55–3.93 μm) alone is enough and the best to detect active fires.

In the following text we present evidence from 330 cases of vegetation fires in NOAA-11/AVHRR images of three continents. Of significant importance, these fires were detected in daytime and not nighttime images, representing the most needed and difficult conditions for their detection. General statistics of the results are given but we concentrate on the main practical problems of fire detection with AVHRR, suggesting techniques toward a global fire product.

Validation of Fires in AVHRR Images

Validation of satellite detection of vegetation fires must rely on known active fires during image acquisition. Prescribed fires or any fires identified during a satellite overpass provide such information; however, due to logistical problems these techniques are limited. The works of Belward et al. (1993) and Setzer et al. (1994), the only known published examples of actual field validation of satellite detection of active fires, reflect the limitations of this method. Another possibility of AVHRR fire validation is cross-comparison with images from high-resolution satellites like the Landsat Thematic Mapper-TM. Pereira Jr. and Setzer (1996) examined new fire scars in a set of three time-consecutive Landsat-TM frames for the same savanna area in relation to the active fires detected with AVHRR

during the same two periods of 16 days for the same area. In the period with best results, 26% of the fires detected by AVHRR could not be verified in the TM images, possibly because they occurred in very short and sparse grasses or because of highly reflective soils or of regrowth caused by rains; 43% of the TM fire scars had no corresponding active fire in the AVHRR image, presumably because these fires were not active during AVHRR imaging or were covered by clouds. Such limitations and the difficulties and the cost of comparing TM and AVHRR images on a worldwide basis limit this approach to a research scale.

In the present work an active vegetation fire in AVHRR images was retained only if it was at the origin of a smoke plume detectable in channel 1 (0.55–0.68 μm) and if simultaneously hot "fire pixels" in channel 3 (3.55–3.92 μm) existed at the same place. Plumes had to show a conical/bending shape typical of fire emissions, with the vortex over the "fire pixels." Fire pixels were those pixels in channel 3 with low digital counts (DN), below 60, which in the inverted scale of channel 3 corresponds to the highest temperature end of the scale. Channel 3 was preferred in relation to other channels because it is the most sensitive to thermal emissions from fires. Smoke plumes were visually detected through digital enhancement of channel 1 images, where they present higher reflectivity in relation to the other AVHRR channels (Pereira and Setzer 1993). The enhancement used was linear stretching, with settings that varied from image to image and according to the region of the images analyzed because of differences in solar illumination, satellite viewing geometry, atmospheric opacity, and background reflectance. Fire pixels were selected using a simple thresholding. Vegetation fires, henceforward also called "fire events," or simply "fires," were selected by overlapping the thresholded channel-3 image with that of channels 1 and applying different linear stretching until plumes could be associated with fire pixels. All processing was done with raw 10-bit resolution uncorrected images. Only images showing at least 10 such independent cases of fire were used in the analyses, and these images were selected after processing hundreds of NOAA-11/AVHRR images of the archives of the Monitoring of Tropical Vegetation Group-MTV at the Joint Research Centre (JRC), Ispra, Italy. Most images presented fewer cases of fires or had no clear, unmistakable association between smoke plumes and fire pixels.

Only AVHRR images of a single satellite, NOAA-11 in this case, were used to avoid the introduction of problems resulting from change of sensors. However, images of different dates along the life of the sensor were used to investigate sensor variations with time. The images concentrated on three regions on different continents where biomass burning is a common feature, and where different types of vegetation are burned. The 33 NOAA-11 images used and the areas covered are listed in table 3.1. Fires in South America included those related to forest conversion in southern Amazonia and in the Pantanal area, and to pasture renewal and agriculture in the savannas/cerrados of central Brazil. In West Africa the fire cases were of forest clearing and savanna burning. For Indochina, in Southeast Asia, fires represented forest conversion, diverse agricultural uses, and savanna burning. The latitudes of the 330 fires analyzed ranged from 28°N to 25°S, thus covering the tropical belt (see table 3.1 for a division of ranges by continent). Being in the north and south hemispheres, the regions studied have their dry, fire season in different periods of the year, and provided diverse sun-target-satellite geometry, thus representing an assorted collection of fire cases and conditions in diverse tropical vegetation ecosystems. For the 330 cases of fires selected, the digital counts of the pixels for a window with 15 lines and 15 columns in the five AVHRR channels centered around each fire were printed and used in the analysis given in the sections below. In some of the windows other fires also existed

Table 3.1 33 AVHRR/NOAA-11 images used in the study for validation of fires in tropical vegetation

	Dates of AVHRR images	Equatorial crossing	Area covered	Latitudes of fires	Longitudes of fires	Original Ecosystems
S	22-Aug -1989	49 W	5N-24S	5-10 S	46-65 W	Fo, TrFo,
	23-Aug -1989	46 W	2N-24S	8-12 S	57-62 W	Fo
A	26-Aug -1989	64 W	0-24S	5-13 S	60-70 W	Fo
M	1-Sep -1989	48 W	2-20S	5-15 S	45-50 W	TrFo, Wo
E	3-Aug -1990	49 W	1-24S	7-23 S	49-57 W	Fo, TrFo
R	4-Aug -1990	46 W	0-24S	7-17 S	45 -54 W	Fo, TrFo
I	11-Aug -1990	52 W	2-24S	11-24 S	49-57 W	Fo, Wo
C	10-Sep -1990	46 W	2-24S	18-21 S	46-55 W	Wo
A	14-Aug -1991	67 W	10-45S	10-24 S	53-64 W	Fo, Wo
	15-Aug -1991	64 W	10-45S	10-24 S	53-63 W	Fo, Wo
W	4-Jan -1989	10 E	2-16N	6-12 N	1 E-12 W	Fo, TrFo, Wo
E	1-Feb -1989	15 E	2-17N	7-12 N	3-14 W	TrFo, Wo
S	4-Feb -1989	12 E	2-17N	6-11 N	5-14 W	Fo, TrFo, Wo
T	21-Feb -1989	15 E	2-16N	5-11 N	5-9.5 W	TrFo, Wo
	23-Dec -1990	07 E	6-21N	6-9 N	4-9 W	Fo, TrFo, Wo
A	26-Dec -1990	02 E	4-19N	7-10 N	1 E-8 W	TrFo, Wo
F	27-Dec -1990	04 E	6-21N	8-12 N	4-1 E	TrFo, Wo
R	28-Dec -1990	07 E	8-22N	9-10 N	2-4 W	Tr Fo, Wo
I	30-Dec -1990	12 E	6-20N	7-9 N	7-9 E	TrFo, Wo
C	31-Dec -1990	10 E	6-21N	9-11 N	3-1 E	Wo
A	2-Dec -1991	03 W	4-19N	7-9 N	7-9 W	TrFo, Wo
	1-Jan -1992	09 E	2-16N	7-11 N	4-14 W	Tr Fo., Wo
	23-Mar -1990	117 E	0-35N	20-25 N	90-95 E	Fo,Wo
	24-Mar -1990	120 E	0-25N	20-25 N	95-105 E	Fo,Wo
S	29-Mar -1990	106 E	7-23N	12-19 N	96-101 E	Fo, Wo
E	30-Mar -1990	109 E	0-25N	15-20 N	97-103 E	Fo, Wo
	17-Apr -1990	109 E	10-15S	12-15 S	130-135 E	Wo
A	25-Mar -1991	102 E	5-25N	10-20 N	98-109 E	Fo, Wo
S	27-Mar -1991	108 E	5-30N	18-22 N	97-104 E	Wo
I	28-Mar -1991	111 E	8-35N	11-22 N	93-108 E	Fo, Wo
A	29-Mar -1991	113 E	15-35N	19-28 N	97-102 E	Wo
	5-Apr -1991	105 E	5-35N	15-20 N	96-100 E	Fo, Wo
	21-Apr -1991	101 E	5-35N	22-28 N	102-108	Fo, Wo

besides the selected fire; they amounted to 294 additional cases and were not eliminated in the analysis in order to make the windows represent typical operational conditions.

Digital Counts or Temperatures?

Digital counts (DNs)in the raw AVHRR images can be converted to albedo values in the case of channels 1 and 2 using prelaunch calibration coefficients. For channels 3, 4, and 5 DN conversion is made either to radiances or to temperatures using on-board calibration values available at each image scan line; these values are measured from a stable blackbody and from space (Kidwell 1991). The saturation temperature for channels 3, 4, and 5 is about 320°K, which is adequate to the temperature ranges of oceans and clouds, the primary targets for which AVHRR was designed; the minimum interval between temperature values is ~0.1°K. According to Wien's displacement law, targets with temperatures in the range of vegetation fires, from 400°C to 700°C, have the maximum of emission from 4.3 μm to 3 μm, resulting in most of the energy concentrated in the band of channel 3 (3.55 μm–3.93 μm). For this reason, and also based on energy emissions from fires in channels 3 and 4 (see following section), our considerations about the use of DNs or temperature/radiances will refer only to channel 3, where the thermal signal from fires is stronger.

Fire pixels in channel 3, regardless of the size of the fire event and of the concentration of biomass burned, are normally not saturated, as shown below (see also Belward et al. 1993; Pereira and Setzer 1993; and Setzer et al. 1994). This fact is against theoretical calculations based on emitted thermal energy which indicate that even a small fire with ~30 m × ~30 m should saturate channel 3 (Robinson 1991). In the 330 cases of fires here analyzed together with the 294 additional cases in the windows, which amounted to 3094 fire pixels, just 54 pixels (1.75%) in 43 cases showed a zero DN, the nominal saturation value of channel 3. So far, the only explanation for this contradictory situation has been proposed by Setzer and Verstraete (1994), who assert that an engineering design problem exists in the on-board processing of the output signal from the channel-3 sensor. According to their hypothesis, signals much beyond the saturation limit of the sensor are indicated with the same values as those of targets below the saturation limit. Figure 3.1 shows the sensor curve proposed to explain why very hot targets like fires or very bright ones like sunglint on water do not saturate channel 3. Regardless of the reasons for this nonsaturation problem, a conceptual question ex-

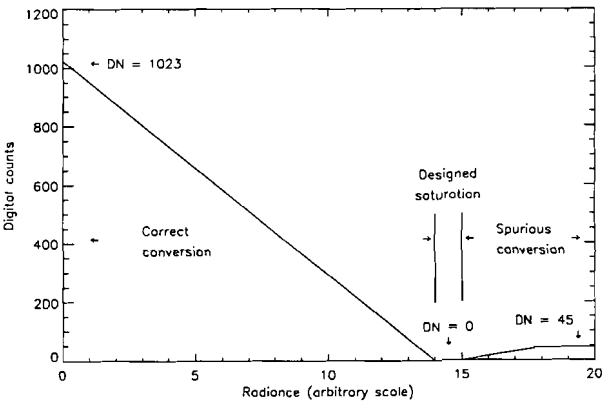

Figure 3.1 Possible explanation for the nonsaturation of channel 3 by fires and highly reflective targets, due to a spurious signal conversion (after Setzer and Verstraete 1993)

ists: what is the meaning of assigning a temperature of ~310°K, therefore below the saturation limit of ~320°K of the sensor, to a target known to have at least some 500°K and which should have saturated the sensor? Our view is that there is obviously a major fault in the conversion of DNs to temperature in the case of fires. With the use of temperatures or radiances instead of digital counts this error possibly increases because the causes and effects of the error are not taken into account in the radiance equations that rely on the DNs. For instance, if the curve suggested in figure 3.1 is correct, the higher the temperature of a fire the lower will be the calculated temperature using current calibration coefficients.

Another strong point in favor of using DNs instead of calculated temperatures or radiances to characterize fire pixels in channel 3 is that fire pixels have DNs about one order of magnitude different from surrounding pixels—see Pereira and Setzer (1993). Any classification algorithm to select fire pixels, based or not on surrounding background values, will be less effective when AVHRR temperatures or radiances are used because the differences are only of a few degrees K.

After Setzer and Verstraete (1994), NOAA modified the AVHRR on NOAA-14 prior to its launch in December 1994, and as a result, hot pixels, such as fires, tend to present full-saturation levels on channel 3 of this sensor. From a fire detection point of view, this change further increased the difficulties in discriminating fires on satellite overpasses during the afternoon.

Which AVHRR Channels?

Detection of active fires in day or nighttime AVHRR images relies on their thermal emissions and therefore only channels 3, 4, and 5 should be considered for this

Table 3.2 Summary of AVHRR digital count values (DNs) for 330 vegetation fires

	channel 2		channel 3		channel 4		channel 5	
	fires	window	fires	window	fires	window	fires	window
averages	156.1	159.9	34.4	414.9	332.1	347.5	290.6	304.4
stand.deviat.	32.0	26.8	8.8	89.5	49.2	42.8	55.9	50.1
maximum	362.0	283.0	50.0	600.0	602.0	575.0	596.0	573.0
minimum	93.5	109.0	1.0	114.0	200.0	227.0	148.0	182.0

purpose. Channels 1 and 2 in daytime images are useful only to see smoke plumes, or to detect fire scars in areas already burned. Nighttime images in the visible part of the spectrum have been used to detect fires on images of the military Defense Meteorological Satellite Program (DMSP) satellites (Cahoon et al. 1992), but the results are contradictory (Langaas 1993) as a possible result of diurnal patterns of burning practices and the difficulty in distinguishing between fires and artificial lights. Table 3.2 summarizes the response of AVHRR channels 2–5 in DNs for the 330 cases of independent vegetation fires selected and also for the corresponding image windows of 15×15 pixels surrounding and including each fire; the total number of fire pixels was 3094, and the total number of pixels in the windows was 74 250. For channel 3 the average values of the fires and the windows were 34.4 and 414.9, respectively, resulting in a ratio of 12 : 1 among them. For channels 2, 4, and 5, the averages of the DNs for the fires and the windows were relatively close.

The average response of channel 3 is still very distinct from that of the windows when the standard deviations of the DNs of the fires are considered: 34.4 ± 8.8 for fires and 414.9 ± 89.5 for the windows (see table 3.2). For channels 2, 4, and 5, the standard deviations of the DNs for both fires and windows indicate no separability at all between fires and their surroundings. Also noticeable in Table 3.2 is that the range of DNs for fires in channel 3 was from 0 to 50, a very small one in comparison to those found in the other channels; the DN average ranges for fires in channels 2, 4, and 5 were 93.5–362, 200–602, and 148–596, respectively. A similar pattern was also observed when the individual fire pixels of each fire event were considered. Also important to note is that the DN range of fire pixels in channel 3, contrary to what occurs in other channels, is not associated to other natural targets, except for highly reflective soils or sun glint. Presenting all data for the 3094 fire pixels, or even to the 330 fire events would require space not available within the scope of this publication, and readers interested in the individual cases should contact the authors.

These observations agree with results from theoretical calculations based on the Planck equation of emissivity as function of wavelengths and temperatures. For the range of channel 3 (3.55 μm–3.93 μm) and assuming emissivity 1, a background surface at 30°C emits close to 0.6 W/m^2 while a fire at 500°C emits 1360 W/m^2, therefore some 2300 times more energy per unit area. For the range of channel 4 (10.35 μm–11.28 μm) the energy emissions at the same temperatures are, respectively, 30 W/m^2 and 510 W/m^2, with the fire emitting 17 times more energy than the background. On the other hand, the area in a pixel actually on fire (i.e., the fire front) is normally small compared to the total pixel area and this situation imposes a limiting effect for fire detection with channel 4. For example, a large fire with a hypothetical continuous front of 500 m by 5 m, or 2500 m^2, occupies only 0.2% of a pixel at nadir with diameter 1260 m. Weighing the emissions in relation to their areas for channel 4, the fire emits the negligible amount of 3.3% of the total energy of the pixel—1.25 million W against 37.3 million W for the rest of the pixel; at off-nadir angles this small percentage is reduced even further. The same situation for channel 3 results in the fire emitting 82% of the total energy of the pixel—3.4 million W against 0.746 million W for the rest of the pixel. Such values together with the curve proposed in figure 3.1 therefore explain why only channel 3 clearly detects the signal from fires, even from small ones. Considering in addition that fires in channel 4 are detected in a very wide range of DNs (200–602), its use in fire detection algorithms is not advisable; the same reasoning is also applicable to channel 5.

Figure 3.2 illustrates these problems by showing DNs cross-sections through two fires; in one case (figure 3.2*a*) channel 4 responds to the signal on channel 3, but in the other case (figure 3.2*b*) the response is the opposite, with channel 4 indicating lower temperature (higher DNs) at the fire pixels than at the nonfire pixels (the DN original scales for channels 3, 4, and 5 are inverted, so that higher counts represent lower temperatures). These fires belong to the same image of 27 March 1991 and are shown in the upper part of the photo of figure 3.5; their distance in columns was 212. Figure 3.3 shows the DNs for the windows surrounding the same two fires which are located in their center. Fire pixels in channel 3 are shown shaded, as well as the corresponding pixels in the other channels; other shaded areas off the center of the window are other fires existing in the same windows. In both cases the difference between fire and nonfire pixels in channel 3 is easily seen as more than one order of magnitude.

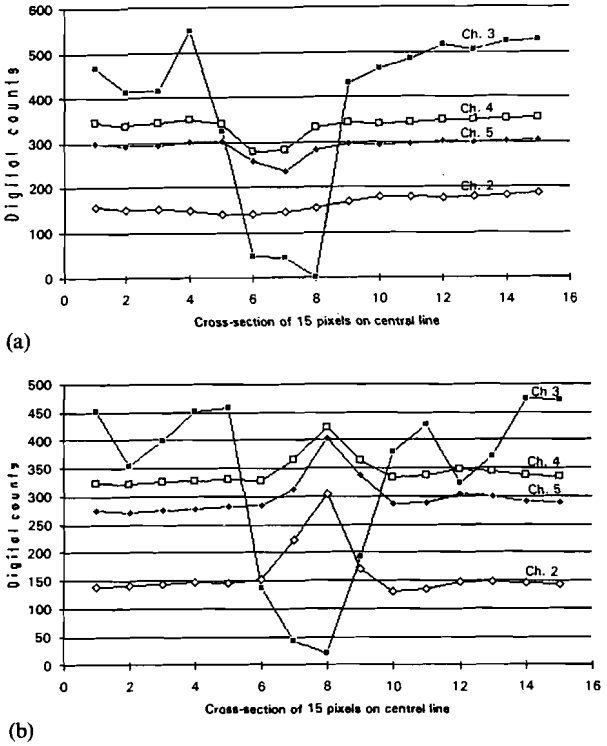

Figure 3.2 The DN cross-section through two fires in AVHRR channels 2–5. In (*a*) channels 3, 4, and 5 respond similarly to the fire, but in (*b*) the response of channels 4 and 5 is inverse. See figure 3.5 for the location of the two fires.

Channel 4 shows a significant reduction in DNs only for the first case but even there the minimum DN observed, 167, was only half of the surrounding nonfire pixels. The relatively high values in channels 1 and 2 in the center of the windows of the two cases result from the high reflectivity of the smoke plumes. The reason for the lower temperatures of channels 4 and 5 in the fire of figures 3.2*b* and 3.3*b* is probably the presence of a much larger smoke plume (see figure 3.5, fires A and B). In both fires the wind blows the plumes to the east and the AVHRR is also to the east. Therefore, with a larger and denser column of smoke in fire B than in fire A, the AVHRR channels 4 and 5 had more difficulty detecting fire B than A, and actually measured characteristics of the plume and not of the fire. The curve and data of channel 2 for fire B (see figures 3.2*b* and 3.3*b*) also shows a strong increase in reflectance from the smoke plume (scale not inverted in this channel) corroborating this interpretation. Channel 3, on the other hand, penetrated smoke to a much larger extent and was not attenuated in this case.

Furthermore, the relation between point temperatures over land and the surface brightness temperature indicated by channels 4 and 5 is not a straightforward one; in many cases, no correlation will even be found (Mansor and Cracknell 1992). This relation can only be estimated if the emissivity of the surface is known and by applying atmospheric correction algorithms based on actual atmospheric profiles of water vapor, aerosols, and temperature for the site of interest at the time of image acquisition—currently an impossible task in terms of available data for tropical regions and of computational needs for a global/regional fire product. Therefore, our suggestion is that channel 3 should be used to detect fires at daytime despite the possible sensor problem shown in figure 3.1 and also of the warning of Kidwell (1991) in the NOAA-series user's guide, page 3-2: "Users should be aware that AVHRR channel 3 data on each TIROS-N series spacecraft have been very noisy due to a spacecraft problem and may be unusable, especially when the satellite is in daylight."

Limitations of Channel 3

Many limitations should be considered when using AVHRR's channel 3 for fire detection. Some of them, already known (Setzer 1993), are: fires not active during the satellite overpass, fire fronts smaller than ~50 m, clouds in the fire-satellite line-of-sight, below canopy fires, and solar reflection. The problem of solar reflection and other limitations are discussed in the following subsections.

Pixel Geometry

The AVHRR resolution is generally referred to as 1.1 km at nadir, and degrading toward the image edges. However, the use of channel 3 for the detection of fires, which are small in relation to the satellite resolution and have a signal one order of magnitude higher than surrounding targets, needs a more thorough analysis. To start with, the instantaneous field-of-view (IFOV) of channel 3 is 0.00151 radians, larger than for other channels; channels 1, 2, 4, and 5 have IFOVs of 0.00139, 0.00141, 0.00141, and 0.00130 radians, respectively (Kidwell 1991). At nadir, considering the satellite at its nominal altitude of 833 km, this corresponds to a circle with a diameter of 1.26 km covering an area of 1.24 km^2. At the image edge the pixel becomes an ellipse with axes of 2.66 km in the along-track direction and 7.25 km in the along-scan direction, and with an area of 15.14 km^2. The interval between any AVHRR consecutive pixels in the same line is 0.0009443 radians, obtained from the scan range of 0.967 radians (55.4 degrees) divided by 1024, the

Channel 01

y \ x	691	692	693	694	695	696	697	698	699	700	701	702	703	704	705
1676	141	137	132	130	131	129	128	128	128	128	129	127	125	124	128
1677	136	132	129	126	129	126	125	126	128	126	128	124	122	144	168
1678	131	130	128	128	126	124	124	125	125	128	127	128	135	160	178
1679	127	128	130	129	124	122	123	122	123	125	141	175	187	203	190
1680	129	126	125	123	123	123	122	128	137	142	173	184	177	199	241
1681	129	128	124	123	124	125	125	155	192	181	192	219	220	217	356
1682	124	123	124	125	126	128	162	198	205	218	213	199	204	270	348
1683	121	122	131	133	128	131	145	146	143	142	136	125	121	120	133
1684	123	140	151	134	121	126	129	122	121	123	122	118	117	117	116
1685	127	158	158	129	116	120	122	120	117	114	114	115	117	122	133
1686	126	130	126	122	121	121	119	117	118	116	114	115	128	154	172
1687	129	128	125	124	123	121	121	118	116	116	115	119	147	164	144
1688	130	128	124	123	123	123	122	118	116	118	118	122	130	120	116
1689	129	128	126	124	124	125	122	118	119	119	117	116	115	114	116
1690	128	127	126	125	127	127	124	121	121	120	118	116	116	116	117

Channel 02

y \ x	691	692	693	694	695	696	697	698	699	700	701	702	703	704	705
1676	154	161	161	160	161	159	156	151	150	150	154	156	158	160	162
1677	153	164	165	161	162	153	150	150	150	148	146	159	164	168	179
1678	165	169	167	161	152	145	145	147	153	149	155	166	171	178	184
1679	160	163	163	156	153	155	156	160	160	157	174	190	191	193	184
1680	160	168	160	152	159	161	163	169	168	153	167	181	179	194	225
1681	158	161	158	155	161	163	166	185	195	176	181	207	208	209	340
1682	154	152	152	156	156	156	173	193	198	209	208	201	211	283	355
1683	157	152	152	148	141	140	145	155	168	178	179	175	179	182	188
1684	155	154	153	140	130	131	147	161	163	160	160	166	174	179	180
1685	163	170	161	153	156	160	158	167	165	160	161	168	174	176	180
1686	163	160	156	162	167	164	159	166	165	163	164	162	167	179	180
1687	160	158	159	164	167	164	164	162	160	163	163	164	169	170	167
1688	157	157	160	164	166	168	167	159	156	160	163	160	160	170	169
1689	157	160	160	166	168	167	163	160	160	164	166	168	169	169	168
1690	156	158	160	160	160	161	163	160	157	158	164	168	167	166	169

Channel 03

y \ x	691	692	693	694	695	696	697	698	699	700	701	702	703	704	705
1676	413	449	481	509	492	500	507	485	476	442	419	427	464	469	446
1677	401	472	484	521	493	485	483	456	440	388	277	400	479	441	418
1678	472	477	495	497	489	481	432	403	422	392	385	454	435	443	495
1679	471	478	443	457	496	504	482	456	448	419	418	445	460	466	478
1680	439	492	470	471	476	495	492	467	431	352	331	425	509	530	512
1681	451	449	468	455	435	423	454	464	491	454	481	502	539	529	372
1682	482	478	446	438	405	104	31	208	475	526	555	545	519	451	351
1683	468	415	414	549	325	46	45	1	430	464	485	517	504	524	526
1684	249	73	289	678	45	46	46	39	445	445	434	491	508	514	525
1685	45	46	45	171	293	1	43	372	490	515	502	494	485	500	526
1686	46	46	45	127	403	385	421	463	483	504	516	416	34	39	468
1687	21	34	104	373	457	459	459	485	505	498	637	43	46	46	16
1688	388	372	409	460	473	491	513	526	505	587	517	46	46	45	461
1689	460	469	449	477	500	480	483	504	498	494	440	348	352	449	511
1690	471	481	491	482	472	470	488	495	467	466	486	477	485	507	516

Channel 04

y \ x	691	692	693	694	695	696	697	698	699	700	701	702	703	704	705
1676	331	334	340	345	342	345	344	336	329	320	312	317	326	323	320
1677	326	333	342	348	343	340	334	325	319	303	292	313	328	322	326
1678	333	337	341	342	340	334	321	315	315	308	311	321	321	329	345
1679	333	335	330	335	342	340	332	324	321	313	317	330	340	348	355
1680	328	340	338	336	338	341	337	330	321	307	314	338	357	371	398
1681	330	332	335	332	331	333	336	342	350	347	355	371	379	400	478
1682	341	337	329	328	327	319	319	339	361	371	375	369	369	410	450
1683	345	339	342	350	341	280	282	331	343	340	344	349	348	351	355
1684	338	337	357	366	313	167	205	324	341	333	332	341	345	347	349
1685	275	151	296	348	347	330	317	339	349	350	343	342	343	348	354
1686	247	80	236	335	339	336	340	344	345	346	344	337	323	335	357
1687	344	338	336	338	340	340	341	348	349	340	335	308	249	291	349
1688	339	337	337	340	342	347	350	351	346	336	323	250	224	316	345
1689	336	336	335	340	344	341	342	344	342	343	342	339	340	347	348
1690	336	338	339	339	336	337	339	340	334	336	339	339	342	347	347

(a)

Figure 3.3 The AVHRR channels 1–4 DN values for windows of two fires located at their centers, but with inverse response in channels 3 and 4. Figures *a* and *b* contain, respectively, the two cross-sections of Figure 3.2. Shaded areas correspond to the fire pixels in channel 3.

Channel 01

y \ x	479	480	481	482	483	484	485	486	487	488	489	490	491	492	493
1704	101	99	99	101	102	104	108	112	117	123	122	131	157	165	154
1705	104	105	107	109	107	109	112	115	117	123	128	141	158	162	158
1706	109	113	114	114	108	109	115	117	115	130	147	144	146	161	163
1707	113	114	113	110	110	114	121	129	134	149	169	159	153	159	161
1708	112	112	110	111	116	124	129	144	173	176	166	156	158	159	161
1709	108	116	117	117	117	139	153	169	186	171	157	158	160	154	154
1710	101	106	113	115	123	160	201	202	157	144	146	156	158	152	148
1711	103	105	108	109	115	138	225	317	180	133	144	166	160	152	151
1712	105	113	114	116	121	130	146	187	161	145	159	187	163	157	168
1713	105	108	112	116	120	122	123	125	125	135	160	164	157	162	163
1714	110	110	110	109	110	113	113	113	114	117	126	137	153	161	155
1715	114	113	111	109	110	112	115	117	117	119	128	161	185	168	144
1716	114	114	114	111	110	112	113	119	120	120	125	179	289	255	193
1717	112	113	115	113	118	125	118	120	120	121	128	158	186	156	142
1718	112	116	116	115	124	132	123	127	136	135	130	130	132	131	134

Channel 02

y \ x	479	480	481	482	483	484	485	486	487	488	489	490	491	492	493
1704	129	136	141	137	139	144	140	143	141	141	136	137	150	160	156
1705	130	135	139	130	129	140	144	148	145	147	141	141	151	155	157
1706	133	136	140	135	130	140	148	150	148	152	150	144	143	148	151
1707	141	140	136	132	128	139	150	150	149	156	160	149	143	143	147
1708	139	141	141	145	144	148	155	155	163	163	155	146	143	145	149
1709	146	151	153	158	149	146	151	157	166	156	146	144	147	146	148
1710	146	151	153	153	149	160	187	180	141	133	133	139	147	146	144
1711	140	142	143	148	145	153	224	304	171	130	135	148	149	145	144
1712	138	138	138	144	150	152	163	196	162	148	159	177	153	148	157
1713	132	136	144	146	149	152	149	145	145	157	173	167	152	156	158
1714	139	140	141	136	137	141	144	142	141	148	155	151	152	160	156
1715	139	133	136	138	138	139	135	136	141	145	151	170	181	169	150
1716	135	133	137	140	142	143	137	138	141	144	145	193	287	253	198
1717	127	133	139	142	144	144	136	137	136	140	151	178	202	174	160
1718	123	134	138	139	141	144	137	139	145	147	146	147	152	152	154

Channel 03

y \ x	479	480	481	482	483	484	485	486	487	488	489	490	491	492	493
1704	326	329	376	375	465	462	442	411	404	396	389	357	368	416	448
1705	350	328	276	247	414	441	373	378	444	422	184	118	370	436	470
1706	349	273	115	215	417	311	38	18	443	444	128	61	392	404	433
1707	386	334	299	330	404	481	98	45	20	454	394	281	443	457	457
1708	335	208	326	420	464	310	432	412	466	472	479	474	482	501	482
1709	401	14	193	506	28	45	42	40	43	323	405	376	473	476	493
1710	446	416	447	434	44	45	43	43	44	120	461	468	466	454	475
1711	451	355	399	452	459	137	42	20	193	380	427	325	371	474	471
1712	400	331	447	461	464	242	169	27	44	119	390	261	257	461	455
1713	438	442	451	475	491	434	156	43	43	359	265	201	345	462	481
1714	403	405	447	435	438	358	373	380	383	362	297	334	366	416	476
1715	434	424	440	445	368	360	411	408	381	395	378	348	372	442	490
1716	392	408	416	427	386	402	391	421	405	410	432	352	228	271	352
1717	348	390	425	442	259	308	401	400	323	394	428	409	395	462	471
1718	281	319	352	422	302	363	411	412	397	369	379	280	256	427	472

Channel 04

y \ x	479	480	481	482	483	484	485	486	487	488	489	490	491	492	493
1704	291	300	304	310	324	321	313	306	303	303	298	294	304	317	325
1705	291	291	289	290	315	319	313	312	313	311	304	302	307	321	330
1706	300	293	288	296	318	323	312	316	320	319	315	311	312	318	325
1707	302	295	296	311	326	332	323	317	327	330	332	330	330	333	332
1708	304	295	305	326	338	334	336	341	347	346	343	340	342	343	337
1709	313	298	312	332	326	313	330	334	332	344	345	344	346	342	338
1710	317	313	319	329	323	325	362	362	323	334	343	345	344	337	334
1711	325	321	326	328	331	329	366	422	363	332	338	349	344	337	336
1712	324	326	329	330	330	325	328	340	314	314	337	353	343	337	343
1713	324	325	326	332	333	323	311	298	294	308	325	330	330	334	340
1714	328	329	324	321	324	320	316	307	301	301	312	317	321	332	340
1715	320	320	323	322	318	315	313	309	302	305	315	345	366	357	347
1716	307	312	317	324	321	312	310	313	309	309	314	353	423	414	369
1717	295	306	319	326	321	316	315	314	309	310	320	345	362	350	337
1718	282	296	315	323	318	318	316	315	311	307	313	324	332	333	332

(b)

Table 3.3 PIxel geometry for AVHRR channel 3 with IFOV = 0.0015rd, satellite altitude of 833 km, and earth radius of 6378 km

Scan Angle (degrees)	Alongtrack Diameter (km)	Alongscan Diameter (km)	Area of Pixel (km2)	Alongscan Pixel dist. (km)	Sat.Pixel Distance (km)	Sat.Px.Cn. Angle (degrees)
0.0	1.26	1.26	1.24	0.79	833.00	180.00
10.0	1.28	1.31	1.31	0.82	847.60	168.68
20.0	1.35	1.46	1.55	0.92	894.28	157.25
30.0	1.49	1.80	2.10	1.13	983.81	145.58
40.0	1.73	2.51	3.40	1.57	1142.82	133.39
45.0	1.91	3.18	4.78	1.99	1267.55	126.92
50.0	2.18	4.36	7.49	2.73	1446.90	119.99
55.4	2.66	7.25	15.14	4.54	1760.82	111.46

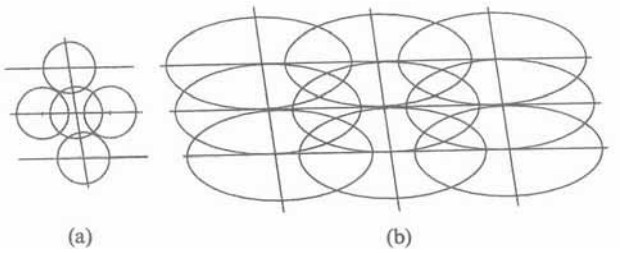

Figure 3.4 Overlap of neighboring channel-3 pixels (*a*) close to nadir and (*b*) at 50° off-nadir. Note that the distance between scan lines remains constant and that the distance between pixels increases proportionally to the along-scan diameter of the pixels; on the other hand, the increase in the along-track diameter causes major pixel overlaps. Pixels drawn in proportion to their dimensions.

number of pixels sampled in the range. At nadir this results in an along-scan distance of 0.79 km between centers of adjacent pixels in the same line; at the image edge, with a satellite-to-pixel distance of 1761 km, this distance becomes 4.54 km. Table 3.3 shows other values for intermediate scan angles. The distance between consecutive scan lines is 1.079 km, assuming the earth to be a sphere with radius 6378 km, the satellite orbit a circle at an inclination of 98 degrees, and 360 scans per minute; this distance is constant in any part of the image.

Therefore, neighboring pixels overlap in any part of the image. At nadir, 51.85% of a channel 3 pixel is also covered by the two neighboring pixels in the same scan line, and an additional 11.47% by the pixels in the neighboring scan lines (see figure 3.4*a*). So, at the minimum no-overlap condition, 36.84% of a pixel is not covered by adjacent pixels. Towards the edge of the image, as shown in figure 3.4*b*, only the percentage overlap from pixels in neighboring lines increases because in the along-scan direction the pixel size increases together with the distance between pixels; in the across-track direction, the distance between pixels, that is between scan lines, remains constant but the pixel across-track diameter increases with its distance from the satellite. At the image edge, almost 100% of a pixel is covered by adjacent pixels and even skipping every other line will still cause some along-track overlap.

Table 3.4 Range of digital counts for AVHRR/NOAA-11 channel-3 fire pixels in 80 cases of vegetation fires (from Setzer and Malingreau 1993)

Date	Region	Case:	1	2	3	4	5	6	7	8	9	10
4-Feb-89	W-Africa	max.	41	41	41	36	39	41	36	41	41	37
		min.	1	5	39	28	39	36	36	10	12	0
		N.Pix	11	11	4	2	2	9	1	9	19	5
26-Aug-89	S-America	max.	43	43	41	43	43	44	43	43	43	42
		min.	25	6	38	3	1	5	4	3	7	11
		N.Pix	14	13	2	4	14	29	8	18	7	4
30-Mar-90	SE-Asia	max.	44	43	43	44	44	45	45	44	44	43
		min.	42	41	4	23	20	23	27	43	0	42
		N.Pix	6	4	11	10	6	12	8	2	4	2
11-Aug-90	S-America	max.	42	48	44	45	45	45	45	45	45	45
		min.	7	0	41	44	41	35	18	38	7	25
		N.Pix	4	20	3	3	5	7	7	15	10	10
31-Dec-90	W-Africa	max.	44	30	44	1	45	35	42	45	45	45
		min.	40	30	44	1	6	19	29	5	20	43
		N.Pix	2	1	2	1	4	2	2	7	5	2
28-Mar-91	SE-Asia	max.	45	26	46	42	45	46	46	46	46	46
		min.	44	19	42	22	44	45	15	43	43	45
		N.Pix	2	2	7	4	2	4	8	6	5	4
15-Aug-91	S-America	max.	47	47	47	47	47	47	47	47	47	47
		min.	37	2	11	33	33	12	2	3	30	22
		N.Pix	8	16	18	8	11	12	56	11	21	12
2-Dec-91	W-Africa	max.	45	47	45	37	45	46	46	47	45	46
		min.	27	17	45	26	42	25	4	41	42	37
		N.Pix	4	11	1	2	2	5	7	8	2	6

The effect of adjacent pixel overlap in channel 3 plays a complex role in fire detection. Depending on its position in the area covered by a pixel, a fire front of ~200 m at nadir can be detected simultaneously in up to three neighboring pixels, each one with 1.24 km^2. At the image edge this same extreme situation can result in the same fire being detected in four neighboring pixels, each with 15.14 km^2. Reduction of this overlap effect could be tried using image deconvolution techniques, but the AVHRR's system modulation transfer functions (MTF) are not available (Breaker 1990) and this possibility remains beyond the scope of the present work.

Degradation of the Sensor

Degradation of the AVHRR channels 1 and 2 was reported for NOAA-11 (Holben et al. 1990), and for NOAAs 7 and 9 (Kaufman and Holben 1993). In the case of channel 3, the existence of on-board calibration data reduces the effects of any sensor response change with time when conversion of radiances or temperatures is applied to the raw data; possibly for this reason no studies of channel 3 variations from other authors are found. Within our view that the use of raw DNs should be preferred for fire detection in relation to radiances and temperatures, any temporal variation in channel 3 will influence detection algorithms. Table 3.4, from Setzer and Malingreau (1993), shows the maximum and minimum pixel DNs for 80 cases of

vegetation fires in 8 images representing almost three years in the life of of NOAA-11. It shows that the maximum DN of fire pixels increases with time, and varied from 41 after the satellite's launch in February 1989, to 46–47 in December 1991. A summary of table 3.4, excluding the DN 48 of the August 1990 image, yields the following temporal variation of channel 3 fire detection limit (Setzer and Malingreau 1993):

Date	DN max
Feb. 1989	41
Aug. 1989	43–44
Mar. 1990	44–45
Aug. 1990	44–45
Dec. 1990	44–45
Mar. 1991	45–46
Aug. 1991	47
Dec. 1991	46–47

Unpublished data from the AVHRR fire detection program in Brazil shows that this DN limit went up further to 48 in August 1992 and to 52 in August 1993. According to this same program, similar variations were observed in past years for the AVHRR channel 3 on-board NOAA-9, thus suggesting that channel-3 degradation with time seems a common feature in the AVHRR series. Therefore, if a fire detection algorithm is entirely or partially based on channel-3 thresholding, the DN value of fire definition has to be checked and adjusted a few times per year. New DN threshold limits for fires are easily found from a histogram of a channel-3 image containing many confirmed fires, that is, with associated well-defined smoke plumes; the DN in the histogram where a sharp peak occurs close to the saturation hot end-of-scale, immediately followed by a discontinuity towards the other end, marks this limit.

Sunglint

Reflections of solar light in water surfaces and highly reflective soils can impose a strong limitation on AVHRR fire detection because they result in the same DNs in channel 3 as fires do (Setzer and Verstraete 1994). Energy from either fires or sunglint reach the satellite at an intensity with the magnitude of $10e^{-9}$ W/m^2. Therefore, channel 3 has a similar sensitivity to reflected light and to fires, being even more sensitive to sunglint than channels 1 and 2. Sunglint occurs in oceans, rivers, lakes, rice paddies, and fish ponds, among others, whenever the sun is close to the plane of the AVHRR swath. The earth stripe parallel to the satellite trajectory which is subject to sunglint is on the order of several hundred kilometers wide by many thousand kilometers long and is found in the left half of images during afternoon ascending orbits. Figure 3.5 illustrates this effect by showing in light gray the Gulf of Siam entirely imaged with sunglint. Because the sun-earth-satellite geometry changes seasonally the sunglint problem is not constant in AVHRR images. For example, the dry/fire season in the central part of South America starts around June when the sun is over the Northern Hemisphere reaching the solstice, and until the equinox of late September no sunglint interferes with fire detection; the same conditions should also prevail for the fire season in South Africa. On the other hand, the detection of fires in Indochina during late March and April at the end or the dry/fire season in that region is strongly impaired by sunglint because at that time the sun is in the Southern Hemisphere, very close to the equator. For all purposes, if a full-year fire product is considered, sunglint will occur at all tropical regions during about one month.

Reflective Soils

Reflective soils also cause very low DNs in channel-3 images, and in many cases the same values associated with fires. Of the total solar energy emitted, only 0.32% is in the range of AVHRR's channel 3; compared to the maximum of 2074 W/m^2-μm at 0.48 μm, only 12 W/m^2-μm reach the earth's surface in the range of channel 3 with zenithal illumination. The reflectance of barren soils, according to the only two references found for channel 3 (Hovis 1966; Suits 1989), vary from 0.13 to more than 0.4. For these values the amount of reflected solar energy reaching the satellite will be of the same order as that from fires and sunglints ($10 \times e^{-9}$ W/m^2), which explains the confusion among these three targets in daytime AVHRR images. Vast areas can be subject to this reflection problem, like all the north of Africa and the Sahel zone in late winter (Grégoire et al. 1993). In the other regions analyzed, this problem was observed only in smaller scales: in the savannas of east central Brazil during October, and in the savannas of northern Indochina and in the Philippines in April. This phenomenon was noticed to be cyclical, occurring and changing its place according to the sun's position like in the case of sunglint from water. Figure 3.5 shows an area of sunglint from land, located close to the east limit of the Gulf of Bengal, and not too distant from an area of major fire activity in the seasonal forest and upland agriculture areas of South China, North

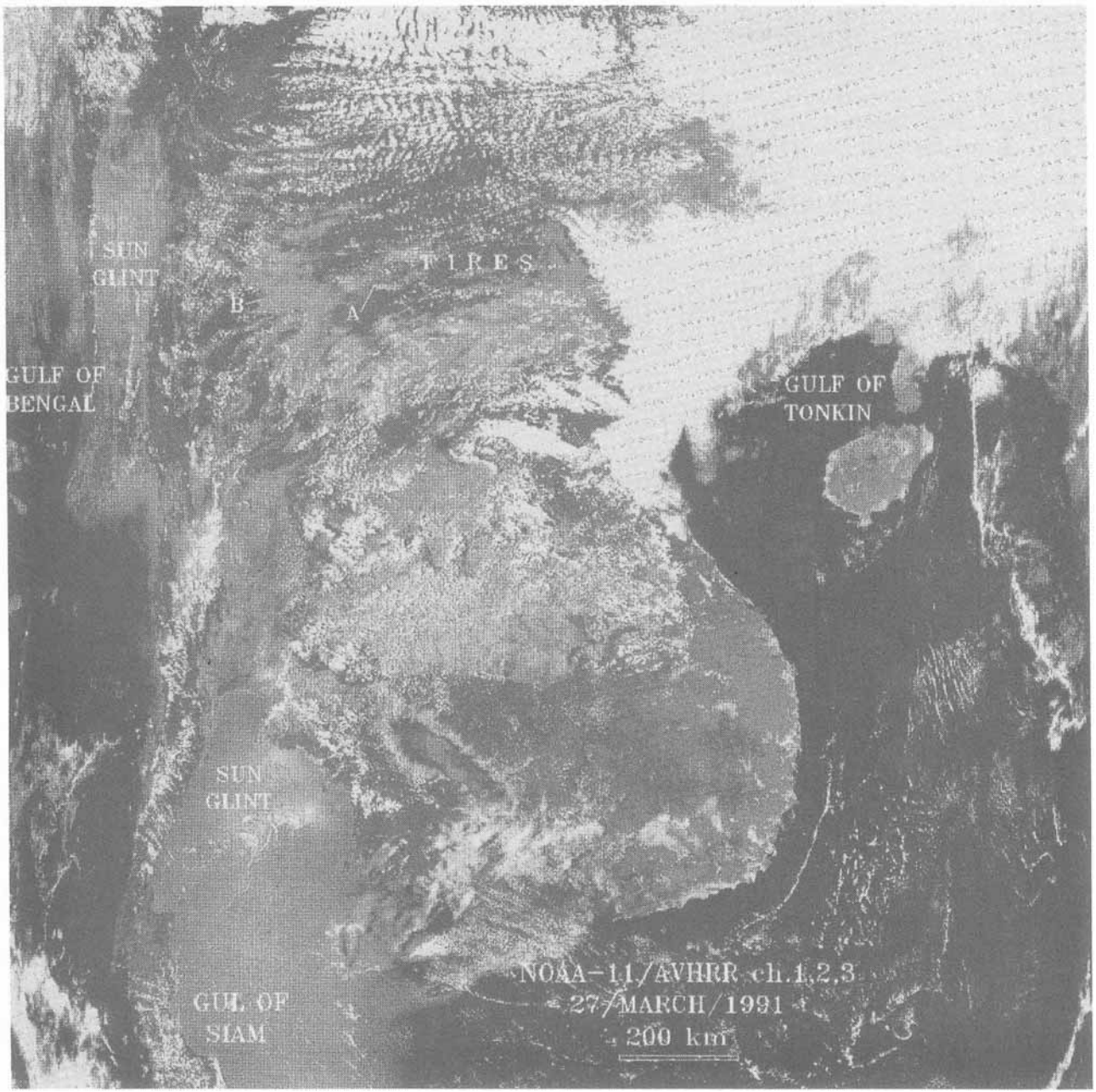

Figure 3.5 The NOAA-11 AVHRR image of Southeast Asia on 27 March 1991 showing major fire activity in its upper part. Strong ocean sunglint occurs in the Gulf of Siam, and land reflection is found east of the Gulf of Bengal. Fires A and B at the origin of large smoke plumes are described in the text.

Vietnam, North Laos, Northeast Birmania, and East Myanmar.

A/D Bit Conversion Problems

Another point to be considered in the detection of fires when channel-3 DNs are used results from imperfect analog-to-digital conversion (A/D) of signals on-board AVHRR. A close examination of a histogram of any AVHRR image of any channel shows peaks and dips occurring at regular intervals in the scale of DN values. These irregularities result from a bias of exactly one DN count in the allocation of DNs in the analog signal of the sensor. In the case of NOAA-11 we observed that this effect is particularly noticed in DN multiples of 8 and 32 in the scale of 0 to 1023, indicating that bits 5 and 7 (where bit 10 is the less significant one) in the A/D are the most deficient ones. As a consequence, for example, an AVHRR histogram will show a discontinuity in which DN 8 shows an excessive number of pixels while DN 7 shows a small number of pixels in relation to the overall trend of the histogram at this range. In this case, many pixels whose analog signal (voltage) nominally corresponds to DN 7 are considered as having the signal of DN 8. The consequence in terms of radiometric resolution is an occasional error of one DN, which is actually the expected precision limit of the AVHRR. In terms of fire detection this implies a faster "degradation" of the sensor when the threshold limit reaches DNs 47 and 55.

Eliminating False Channel-3 Fires

Figure 3.5 is a good example of a critical and real situation where sunglint in an AVHRR image must be eliminated in order to allow proper identification of active fires; without any screening most of the Gulf of Siam and parts of land in the upper left corner of the image would be erroneously classified as fires in channel 3 together with the many hundreds of real vegetation fires also present in the image. The most simple and practical automatic way to minimize sun reflection in channel-3 fire detection is the use of the latest of possible multiple and consecutive AVHRR overpasses that cover the region subject to sunglint or to soil reflection. With this technique an area in the west half of an image with specular reflection will be imaged at a very large scan angle towards the east in the next orbit. At equatorial latitudes this possibility is restricted only to regions at off-nadir scan angles larger than 44°, and just for 3 out of every 9 days—the orbital repetition cycle of the NOAA-series satellites. At latitudes of 30° multiple coverage can be extended to scan angles larger than 38° during 4 out of every 9 days. A good illustration of these repetition patterns in consecutive orbits is found in Goward et al. (1991), while Gutman (1991) shows the 9-day periodicity of scan angles for a single location. Orbital prediction programs combined with calculations of sun-target-satellite geometry can be used to exclude sunglint areas from the fire-detection procedures in areas subject to sun reflection that can not be re-imaged in no-sunglint conditions.

Another possibility to exclude sunglint is the use of masks following contours of continents and main rivers. However, this is restricted only to large bodies of water; in addition, maps and navigation imprecisions will always cause a considerable amount of errors along even the main bodies of water. A third option is the combination of multiple AVHRR channel data. In most cases channels 4 and 5 will show no response at all for fires. Their use to determine if sun reflection is occurring is also very limited because both fires and reflection can occur in a background of relatively high or low temperatures. For example, in the same image of South America sunglint is found in the high peaks and dry salt lakes of the Andes mountains in a below-freezing temperature background and also in a 30°C environment in Brazilian cerrados. If thin clouds or smoke cover the region these channels may not penetrate them when channel 3 does and the temperature indication they will produce will not make sense in terms of fire detection. Channels 1 and 2 are probably the best ones to eliminate sun reflection. The key in this option is to select the correct thresholding value because it will vary with the sun-pixel-satellite geometry; bidirectional reflectivity equations may be thus used and account for variations of solar illumination. As in channels 4 and 5 thin clouds and smoke plumes over fires will cause errors because in this case either channel 1 or 2 will consider a fire as sunglint.

A last possibility to identify sun reflection can be considered. Fires are usually limited to a few contiguous pixels, while sun reflection is associated with hundreds or even thousands of contiguous pixels; for the total of 624 cases of fires in this study (330 cases selected and 294 others in the windows), the average was 4.96 fire pixels per fire. Therefore a simple algorithm that checks the number of pixels in the spatial distribution of fire pixels in channel 3 could eliminate sun reflections in most cases.

A global product of AVHRR full-resolution images involves very large amounts of data processing since one such composite image has $\sim$1.4 gigabytes per

channel. Having in mind the shortest possible computing demand for a global fire product, our initial tentative suggestion for detecting real fires and eliminating false fires in channel 3 caused by sun reflection is basically the following:

- Mask out oceans, seas, and large lakes in the processing of images.
- If a region is subject to sun reflection, try the use of the consecutive orbit for that region.
- Use simple thresholding to select hot/fire pixels in channel 3.
- For each fire pixel detected in channel 3, check the corresponding pixel value in channel 1 to eliminate strong glint cases; if the value in channel 1 is above a specific (bright) threshold for that part of the image, reject the pixel as a fire pixel.
- If the pixel value in channel 1 is below the specific (dark) threshold, check the spatial distribution of fire pixels in channel 3; for less than ~ 20 contiguous pixels, accept the fire event; otherwise reject it as a fire.

And finally, an effect that reduces sunglint and is provided by orbital variations of the afternoon pass of NOAA satellites must be mentioned. Although called sun-synchronous the equatorial crossing time of these satellites varies gradually from their launching dates, resulting in a drift, or delay, of about 20 minutes per year. The resulting change in the sun-earth-satellite geometry with a lower sun in the sky significantly shifts the sunglint toward the left edge of the images, improving fire detection in the more central part of the image.

Border Effects

Usually AVHRR analyses discard information from pixels beyond a scan angle of ± 30 degrees to avoid the use of large pixels and to minimize atmospheric optical effects. This is not necessary in the case of fire detection using channel 3. The size of a pixel does not interfere with fire detection because the energy emitted even by small fires (fire front larger than ~ 50 m) is enough to reach the fire detection limit regardless of the pixel size. At the 3.75-μm band range atmospheric transmittance is about 90% (LaRocca 1989), higher than for any other part of the spectrum (in the visible and near-infrared parts it is $\sim 60\%$). This makes channel 3 less sensitive to atmospheric attenuation, even at large-scan angles with longer slant distances (for the limit scan angle of 55.4° the air mass is ~ 2.7 times the zenith air mass). It is also much less sensitive to haze by a factor of 30–200 times compared to channel 1 in the 0.64-μm band (Kaufman and Remer 1994). This last characteristic is of particular importance in off-nadir fire detection since regions subject to intense biomass burning are covered by dense smoke palls of millions of km^2 (see Andreae et al. 1988; Helfert and Lulla 1990; Setzer and Pereira 1991b). Many of the 330 cases of fires analyzed here were purposely selected very close to the image borders in order to find out if they presented any particular radiometric or spatial patterns. Most of them were in the column range of 0 to 100 in relation to the borders at scan angles larger than 50°, with an extreme case at column 5 and 55.13° off-nadir. One of the cases had just one fire pixel associated, but most of the others presented a distribution more elongated in the across-track direction, as expected from the considerations presented above. As in central parts of the images smoke plumes in the edges of the images also had channel-3 fire pixels at their origin within the same DN limit as for the rest of the image, thus indicating that channel-3 fire detection can be extended to the full image. The only constraint is the loss of geographical precision in the location of fires because of the larger size of pixels at the image edges.

Geometric Corrections

Because of the NOAA satellite's low altitude of ~ 830 km and the radiometer scanner wide-angle coverage of $\pm 55°$, the off-nadir geometry of pixels is distorted, becoming an ellipse of 2.7 km $\times$ 7.3 km at the image edges for channel 3. AVHRR geometrically corrected images are referenced to a base of pixels with constant size forcing the correction algorithm to repeat and interpolate original pixel values to obtain corrected pixels. Fire fronts are usually restricted to very small areas relative to the AVHRR resolution and most fires are indicated by a few contiguous pixels. Therefore, after geometric correction the number of fire pixels in a particular fire event will differ from that in the original image. This effect is illustrated in table 3.5, where the same 10 fire events in one AVHRR image were compared in their raw and geometrically corrected forms. The table shows that for large off-nadir angles, as in the last two cases, the number of fire pixels can double in the corrected image. In terms of ground-surface equivalence of fire pixels both types of images present similar results, but for characterizing individual fires the corrected image introduces additional difficulties. For example, one isolated fire pixel in a raw image indicates a fire front between ~ 50 m

Table 3.5 Effect of geometric correction in the number of fire pixels for the AVHRR image of 15 August 1991. Fires are listed in sequence of off-nadir angles.

Raw image				Geometr.corrected image		
Off-nadir angle	No.Fire pixels	Maxim. DN	Minim. DN	No.Fire pixels	Maxim. DN	Minim. DN
7.5	16	47	2	13	47	2
9.0	8	47	37	6	47	37
16.4	18	47	11	17	47	11
18.2	57	47	2	53	47	2
21.7	21	47	30	18	47	30
22.9	12	47	22	11	47	22
23.8	11	47	3	9	47	3
28.2	12	47	12	13	47	12
48.1	11	47	33	23	47	33
48.3	8	47	33	20	47	33

and a few hundred meters long, most likely from just one fire. If in the corrected image two or more fire pixels are produced for the same fire, the same interpretation about its size cannot be made; in this case the possibility of two or more independent but close fire events has to be considered. This difficulty increases for mosaics composed of many corrected AVHRR images, causing random modifications in the number of fire pixels. For fire pixels close to nadir the effect of correction may actually reduce the number of fire pixels, as seen in table 3.5. In this case, for fires associated with few pixels the risk exists that important information like the minimum or maximum value of the fire pixels is lost in the transformation of images. Our suggestion towards a global composite product is that raw unprocessed images be used to reduce loss or modification of information, and the number of fire pixels in grid cells be updated on a daily basis if possible. If the objective is the real-time combat of fires, then the geographical coordinates of fire pixels in the raw images should be used.

8-Bit or 10-Bit Images?

The AVHRR images are transmitted by the NOAA-series satellite and received by ground stations on a 10-bit/1024-level radiometric scale. However, some image-processing systems operate on an 8-bit/256-level scale configuration either to speed up processing or to fit internal software and hardware requirements; as a result AVHRR image conversion to 8-bit resolution is common. This conversion is usually achieved by dropping the two less significant bits in the 10-bit data, or by dividing 10-bit values by 4 and giving the result as a round number. As shown above, fires are better detected in channel 3, up to a very specific and precise count level, which changes in the satellite's life. If the conversion to 8-bit is made, this distinction becomes more difficult and errors in the selection of fire pixels may occur. For example, if the threshold detection is 0–46 in the 0–1023 scale, it will correspond to the range 0–11 on a 0–256 scale when the two least significant bits are dropped or to the range 0–12 if division by 4 with rounding is used. In the first case the eleventh level includes original counts 44–47, and in the second case the twelfth level includes the counts 46–49. The upper limit in both cases does not correspond to the exact fire threshold detection and may include values not associated with fires. Therefore, 10- to 8-bit conversion should be avoided in AVHRR fire detection whenever possible.

Another problem may occur in the 10- to 8-bit conversion, and is caused by badly designed software, as was the case in a system used worldwide that we tested at the start of the present work. Unsound as it may seem, in this case the conversion is done by dropping the two most significant bits instead of the two less significant ones. One of the symptoms caused by this error is that badly converted channel-3 images present many pixels at the cold saturation extreme of the scale with DN = 255; unfortunately, publications in the literature contain this mistake.

Conclusions

The use of NOAA/AVHRR 1.1 km resolution images for fire detection in different tropical ecosystems of the world and in diverse imaging conditions was analyzed in the perspective of developing a global fire product. The principal contribution of this analysis is the recommendation of the use of channel 3 as the main channel for fire detection anywhere and at any time; in particular, its DNs should be used instead of any derived radiative parameter information. Although this channel presents inaccurate response to fires due to a sensor engineering problem, it is this very problem that fortuitously allows a clear identification of fire spectral signatures. The main constraint in its use at daytime is solar reflection from exposed reflective soils and from water surfaces; to minimize it the combined use of channel 1 and of a spatial analysis of fire pixels is recommended. Because the energy seen by the satellite in fires or reflections has about the same magnitude, the resulting misidentification of targets is expected to occur in satellites with sensors of higher resolution operating in the 3–4 μm solar spectrum region.

Other limitations of channel 3 in fire detection presented and analyzed were excessive overlap of neighboring pixels causing repetition of fire detection; degradation of the sensor along the years, which require updates in fire detection thresholds; and slight

misreading of one DN in the on-board analog-to-digital conversion. In a global fire product, these limitations have to be considered together with already known ones such as: fires not active during satellite overpasses, fire fronts smaller than ~50 m, clouds in the fire–satellite line of sight, and fires not reaching the canopy. Combined effects of these fire-related factors have been reviewed and evaluated in Malingreau (1990).

Notwithstanding many limitations in the use of high-resolution AVHRR images, a global fire product is attainable and its production should be started at the earliest possible time. No other source of data in the next years will provide regular and consistent world-wide detection of fires.

Acknowledgments

We acknowledge the support of the Brazilian Scientific Council (CNPq) which made the development of this work possible through grant no. 200602/79-9. A. S. Belward, J. M. Grégoire, and P. Kennedy were very helpful in discussions of fire detection and their location in the AVHRR images; G. de Souza assisted with image-processing hardware and software.

References

Andreae, M. O. 1993. Global distribution of fires seen from space. *EOS Transact., AGU*, 74(12):129, 135.

Andreae, M. O., Browell, E. V., Garstang, M., Gregory, G. L., Harris, R. C., Hill, G. F., Jacob, D. J., Pereira, M. C., Sachse, G. W., Setzer, A. W., Silva Dias, P. L., Talbot, R. W., Torres, A. L., Wofsy, S. C. 1988. Biomass Burning Emissions and Associated Haze Layers Over Amazonia. *J. Geophy. R.*, 93(D2):1509–1527.

Belward, A. S., Grégoire, J.-M., D'Souza, G., Trigg, S., Hawkes, M., Brustet, J.-M., Serca, D, Tireford, J.-L., Charlot, J.-M., and Vuattoux, R. 1993. In-situ, real-time fire detection using NOAA/AVHRR data. *Proc., 6th AVHRR User's Conf.*, Belgirate, Italy, 28 June–2 July; Eumetsat/Joint Research Centre 333–339.

Breaker, L. C. 1990. Estimating and removing sensor-induced correlation from advanced very high resolution radiometer satellite data. *J. Geophys. Res.*, 95(C6):9701–9711.

Cahoon, D. R., Stocks, B. J., Levine, J. S., Cofer, W. R., O'Neill, K. P. 1992. Seasonal distribution of African savanna fires. *Nature*, 359:812–815.

Crutzen, P. J., Heidt, L. E., Kranec, J. P., Pollock, W. H., and Seiler, W. 1979. Biomass burning as a source of atmospheric gases CO, H_2, N_2O, NO, CH_3Cl, and COS. *Nature*, 282:253–256.

Crutzen, P. J. and Andreae, M. O. 1990. Biomass burning in the tropics: impact on atmospheric chemistry and biogeochemical cycles. *Nature*, 250:1669–1678.

Crutzen, P. J. and Goldammer, J. G. 1993. *Fire in the Environment: The Ecological, Atmospheric, and Climatic Importance of Vegetation Fires*. Chichester, John Wiley, 497 pp.

Goldammer, J. G. 1993. Historical biogeography of fire: tropical and subtropical. In *Fire in the Environment: Its Ecological, Climatic, and Atmospheric Chemical Importance*, Eds. P. J. Crutzen and J. G. Goldammer, chap. 15, pp. 297–314. New York, John Wiley.

Goward, S. N. Markham, B., Dye, D. G., Dulaney, W., and Yang, J. 1991. Normalized difference vegetation index measurements from the advanced very high resolution radiometer. *Remote Sens. Environ.*, 35:257–277.

Grégoire, J. M., Belward, A. S., and Kennedy, P. 1993. Dynamiques de saturation du signal dans la bande 3 du senseur AVHRR: Handicap majeur ou source d'information pour la surveillance de l'environnement en milieu soudanoguinéen d'Áfrique de l'Ouest? *Int. J. Remote Sensing*, 14 (11):2079–2095.

Gutman, G. G. 1991. Vegetation indices from AVHRR: an update and future prospects. *Remote Sens. Environ.*, 35:121–136.

Helfert, M. R. and Lulla, K. P. 1990. Mapping continental-scale biomass burning and smoke palls over the Amazon Basin as observed from the Space Shuttle. *Photogram. Eng.*, 56(10):1367–1373.

Holben, B. N., Kaufman, Y. J., and Kendall, J. D., 1990. NOAA-11 AVHRR visible and near-IR inflight calibration, *Int. J. Remote Sensing*, 11, 1511–1519.

Hovis, W. A. Jr. 1966. Infrared spectral reflectance of some common minerals. *Applied Optics*, 5(2):245–248.

IGBP. 1992. Improved global data for land applications: a proposal for a new high resolution data set. Ed. J. R. G. Townsend, *International Geosphere and Biosphere Program—IGBP*, Report 20, Stockholm.

Kaufman, Y. J. and Remer, L. A. 1994. Detection of forests using mid-IR reflectance: an application of aerosol studies. IEEE *J. Geosc. and Rem. Sens.*, 32:672–683.

Kidwell, K. B. 1991. *NOAA Polar Orbiter Data User's Guide*. NOAA/NESDIS, Washington, D.C.

Langaas, S. 1993. Diurnal cycles in savanna fires. *Nature*, 363, 120.

LaRocca, A. J. 1989. Atmospheric absorption. In *The Infrared Handbook*, Eds. W. L. Wolfe and G. J. Zissis, pp. 5.1–5.132 (Ann Arbor, MI; E.R.I.M.).

Levine, J. S. 1991. *Global Biomass Burning: Atmospheric, Climate, and Biospheric Implications*. MIT Press, Cambridge, Mass., 569 pp.

Malingreau, J. P. 1990. The contribution of remote sensing to the global monitoring of fires in tropical and subtropical ecosystems. In *Fire in the Tropical Biota*, Ed. J. G. Goldammer, chap. 15, pp. 337–370. *Ecosystem Processes and Global Challenges, Ecological Studies*. Springer-Verlag, Berlin-Heidelberg.

Malingreau, J. P., Albini, F. A. Andreae, M. O., Brown, S., Levine, J., Lobert, J. M., Kuhlbush, T. A., Radke, L., Setzer, A., Vitousek, P. M., Ward, D. E. and Warnatz, J. 1993. Group report: quantification of fire characteristics from local to global scales. In *Fire in the Environment: Its Ecological, Climatic, and Atmospheric Chemical Importance*, Ed. P. J. Crutzen and J. G. Goldammer, chap. 19, pp. 327–343. New York, John Wiley.

Mansor, S. B., and Cracknell, A. P. 1992. Land surface temperature from NOAA-9 AVHRR data. *Proceedings, 18th Annual Conf. of the Remote Sensing Society*. Ed. A. P. Cracknell and R. A. Vaughan. The Remote Sensing Society. University of Dundee, 15–17 Sept. 1992; pp. 274–286.

Matson, M. and Dozier, J. 1981. Identification of subresolution high temperature sources using thermal IR sensor. *Photogram. Engin. and Remote Sensing*, 47:1311–1318.

Pereira, Jr., A. C, and Setzer, A. W. 1996. Comparison of fire detection in savannas using AVHRR's ch. 3 and TM images, *Int. J. Remote Sens.*, 17(10)1925–1937.

Pereira, M. C. and Setzer, A. W. 1993. Spectral characteristics of deforestation fires in NOAA/AVHRR images. *Int. J. Remote Sensing*, 14(3):583–597.

Robinson, J. M. 1991. Fire from space: global fire evaluation using infrared remote sensing. *Int. J. Remote Sensing*, 12(1):3–24.

Setzer, A. W. 1993. Operational monitoring of fires in Brazil. *Internat. Forest Fire News*, 9:8–11.

Setzer, A. W. and Pereira, M. C. 1991a. Operational detection of fires in Brazil with NOAA/AVHRR. *24th. Internat. Symp. on Remote Sensing of the Environment*, Rio de Janeiro, Brazil (Ann Arbor, E.R.I.M.), 469–482.

Setzer, A. W. and Pereira, M. C. 1991b. Amazonia biomass burning in 1987 and an estimate of their tropospheric emissions. *Ambio*, 20(1):19–22.

Setzer, A. W. and Malingreau, J. P. 1993. Temporal variation in the detection limit of fires in AVHRR's ch. 3. *Proc. 6th AVHRR User's Conf.*, Belgirate, Italy, 28 June–2 July, Eumetsat/Joint Research Centre, pp. 575–579.

Setzer, A. W. and Verstraete, M. M. 1994. Fire and glint in AVHRR's ch. 3: a possible reason for the nonsaturation mystery. *Internat. J. Remote Sensing*, 15(3):711–718.

Setzer, A. W., Pereira Jr., A. C. and Pereira, M. C. 1994. Satellite studies of biomass burning in Amazonia: some practical aspects. *Remote Sensing Reviews*, 10:91–103.

Singh, K. D. 1993. The 1990 tropical forest resources assessment. *Unasylva/FAO*, 44(174):10–19.

Suits, G. H. 1989. Natural Sources. In *The Infrared Handbook*, Ed. W. L. Wolfe and G. J. Zissis, MI, pp. 3.1–3.154 (Ann Arbor, E.R.I.M.).